GFZ
Helmholtz-Zentrum
POTSDAM

Originally published as:

Amm, O., Vanhamäki, H., Kauristie, K., Stolle, C., Christiansen, F., Haagmans, R., Masson, A., Taylor, M. G. G. T., Floberghagen, R., Escoubet, C. P. (2015): A method to derive maps of ionospheric conductances, currents, and convection from the Swarm multisatellite mission. - *Journal of Geophysical Research*, *120*, 4, pp. 3263–3282.

DOI: http://doi.org/10.1002/2014JA020154

AGU PUBLICATIONS

JGR

Journal of Geophysical Research: Space Physics

TECHNIQUE

10.1002/2014JA020154

Key Points:
- A new method for analyzing data by the Swarm satellites of European Space Agency
- Producing local maps of auroral electromagnetic fields currents and conductances
- Estimation of *K* parameter from ionospheric and magnetospheric data analysis

Correspondence to:
K. Kauristie,
Kirsti.Kauristie@fmi.fi

Citation:
Amm, O., H. Vanhamäki, K. Kauristie, C. Stolle, F. Christiansen, R. Haagmans, A. Masson, M. G. G. T. Taylor, R. Floberghagen, and C. P. Escoubet (2015), A method to derive maps of ionospheric conductances, currents, and convection from the Swarm multisatellite mission, *J. Geophys. Res. Space Physics*, *120*, 3263–3282, doi:10.1002/2014JA020154.

Received 7 MAY 2014
Accepted 4 MAR 2015
Accepted article online 9 MAR 2015
Published online 13 APR 2015

A method to derive maps of ionospheric conductances, currents, and convection from the Swarm multisatellite mission

O. Amm[1,2,3], H. Vanhamäki[1,4], K. Kauristie[1], C. Stolle[5,6], F. Christiansen[5], R. Haagmans[7], A. Masson[8], M. G. G. T. Taylor[7], R. Floberghagen[9], and C. P. Escoubet[7]

[1]Finnish Meteorological Institute, Helsinki, Finland, [2]Solar-Terrestrial Environment Laboratory, Nagoya University, Nagoya, Japan, [3]Deceased 16 December 2014, [4]Now at Astronomy and Space Physics Unit, University of Oulu, Oulu, Finland, [5]Astrophysics Division, Technical University of Denmark, DTU Space, Lyngby, Denmark, [6]Now at Astronomy and Space Physics Unit Helmholtz-Centre Potsdam, GFZ German Research Center for Geosciences, Potsdam, Germany, [7]European Space Agency/ESTEC, Noordwijk, Netherlands, [8]European Space Agency/ESAC, Madrid, Spain, [9]European Space Agency/ESRIN, Frascati, Italy

Abstract The European Space Agency (ESA) Swarm spacecraft mission is the first multisatellite ionospheric mission with two low-orbiting spacecraft that are flying in parallel at a distance of ~100–140 km, thus allowing derivation of spatial gradients of ionospheric parameters not only along the orbits but also in the direction perpendicular to them. A third satellite with a higher orbit regularly crosses the paths of the lower spacecraft. Using the Swarm magnetic and electric field instruments, we present a novel technique that allows derivation of two-dimensional (2-D) maps of ionospheric conductances, currents, and electric field in the area between the trajectories of the two lower spacecraft, and even to some extent outside of it. This technique is based on Spherical Elementary Current Systems. We present test cases of modeled situations from which we calculate virtual Swarm data and show that the technique is able to reconstruct the model electric field, horizontal currents, and conductances with a very good accuracy. Larger errors arise for the reconstruction of the 2-D field-aligned currents (FAC), especially in the area outside of the spacecraft orbits. However, even in this case the general pattern of FAC is recovered, and the magnitudes are valid in an integrated sense. Finally, using an MHD model run, we show how our technique allows estimation of the ionosphere-magnetosphere coupling parameter *K*, if conjugate observations of the magnetospheric magnetic and electric field are available. In the case of a magnetospheric multisatellite mission (e.g., the ESA Cluster mission) several *K* estimates at nearby points can be generated.

1. Introduction

The derivation of field-aligned currents (FAC) from low-orbiting satellite data was one of the focus interests from the very beginning of scientific satellite missions. The most famous result of the early missions was the discovery that the auroral region is covered by two meridionally separated FAC sheets that have opposite polarity in the premidnight as compared to the postmidnight sector [*Zmuda and Armstrong*, 1974; *Iijima and Potemra*, 1976]. The technique to derive the FAC from satellite magnetometer data was based on the assumption of an infinite, straight FAC current sheet that is aligned along the zonal direction. In this case, the FAC density is directly proportional to the meridional gradient of the zonal disturbance magnetic field component. Slightly modified versions of this technique have been used in numerous studies [e.g., *Iijima and Potemra*, 1978; *Rich and Gussenhoven*, 1987; *Fujii et al.*, 1994]. The impacts of the current sheet not being infinite in reality, as well as of a tilt with respect to zonal direction, have been studied by *Fung and Hoffman* [1992].

In addition to FAC, the distribution of the horizontal ionospheric currents is often a useful parameter to be analyzed. *Olsen* [1996] developed a technique to estimate this parameter from low-orbiting satellite magnetic data, under the assumption of infinitely long, straight, east-west directed horizontal currents. However, using that same data set the results of this technique will typically not match with the results of the traditional technique to determine FAC as mentioned above, in the sense that the divergence of the derived horizontal currents will not be equal to the independently derived FAC. This is due to the fact that usually the FAC flow much closer to the satellite than the horizontal ionospheric currents do, and thus when using independent analysis techniques for the two current components, the results will contain information of different spatial scales. This problem is avoided when using techniques that match both the

©2015. American Geophysical Union. All Rights Reserved.

FAC and the horizontal currents simultaneously, such as those based on Spherical Elementary Current Systems (SECS), first introduced by *Amm* [1997]. For the use of this technique with single-satellite data, a one-dimensional variant of the general SECS approach (1-D SECS) has been used [*Vanhamäki et al*., 2003; *Juusola et al*., 2006]. In this variant, in contrast to the general approach (also called 2-D SECS), a horizontal direction needs to be specified in which gradients are vanishing. The 1-D SECS approach allows checking from the satellite magnetic data themselves whether or not such a condition is applicable to given limits for a specific situation. It also allows finding the direction for which this condition is optimally satisfied. This direction does not need to be perpendicular to the satellite track. The horizontal currents and FAC derived from this technique are by definition always consistent with each other. Moreover, the horizontal currents are also not straight, but flowing along the spherical surface of the ionospheric current layer. The 1-D SECS technique has successfully been applied to an extensive set of magnetic field data from the CHAMP satellite mission [*Reigber et al*., 2002], both for individual event and for statistical analysis [e.g., *Ritter et al*., 2004; *Juusola et al*., 2007].

In this paper, we extend the aforementioned technique for the case that two (or more) low-orbiting satellites are flying in constellation. We also take into account the opportunities that arise when these satellites measure not only the magnetic but also the electric field (or equivalently, plasma convection). This is the case for the recently launched Swarm satellite mission [*Olsen et al*., 2013], consisting of a pair of near-polar orbiting satellites at about 480 km altitude, which are flying in a parallel constellation separated by 1.4° longitude at the equator, and one near-polar orbiting satellite at about 510 km. The orbital plane of the upper satellite will rotate with respect to the lower satellite pair such that after about 3 years of operation, the angle between the two planes will be 90°. The nominal lifetime of the mission is 4 years. While the technique presented in this paper was developed with the Swarm mission in mind, we emphasize that it can be applied to any low-orbiting multisatellite mission with nearby spacecraft carrying magnetic and electric field instruments.

The basic idea of the new technique presented here is to use 1-D and 2-D SECS simultaneously, in order to derive spatial maps of ionospheric electrodynamic parameters in between, and to some extent even outside of the orbits of the two parallel flying satellites. Given the magnetic and electric field measurements of the satellites (in this paper synthesized from models), we derive these spatial maps not only for horizontal currents and FAC but also for the electric field/plasma convection and the ionospheric Hall and Pedersen conductances. Such maps allow studying spatial gradients of these parameters in any horizontal direction. To our knowledge, this is the first time that spatial maps of such parameters are generated from (presently synthetic) electromagnetic observations of low-orbiting satellites. In particular, maps of ionospheric conductances for specific events are very difficult to obtain with other techniques and require a combination of data sets from different instruments, which are not often available [cf. *Vanhamäki and Amm*, 2011]. Further, we present an approach for estimating the ionosphere-magnetosphere coupling parameter K [e.g., *Yoshikawa et al*., 2011, and references therein], when conjugate magnetospheric magnetic and electric field data are also available. The K parameter corresponds to an integrated field-aligned conductivity between the magnetosphere and the ionosphere and is thus a crucial parameter for quantifying the coupling between the two regions. The technique presented in this paper is, in its current state, applicable to the auroral region but not to the midlatitudes or to the equatorial region.

Section 2 presents the analytical basis of the new technique, as well as the fundamental geometrical layout for its application. Section 3 then gives several application examples for the technique, based on synthetic test cases. These test cases include models of ionospheric electrodynamics situations for testing the new low-orbiting multisatellite analysis technique, as well as a test case for the K parameter estimation based on a situation generated by an MHD model. Finally, the performance of the technique is discussed in section 4, and a summary is presented.

2. Technique

In this section we briefly present the analytical background of our new analysis technique for deriving maps of ionospheric parameters from electric and magnetic field data of multiple low-orbiting satellites and for estimating the magnetosphere-ionosphere coupling parameter K. The basis functions used for the first part of this analysis are Spherical Elementary Current Systems (SECS). These basis functions consist of two sets of vector fields on the sphere, which are Green's functions of the curl and divergence operators in spherical geometry, respectively.

©2015. American Geophysical Union. All Rights Reserved.

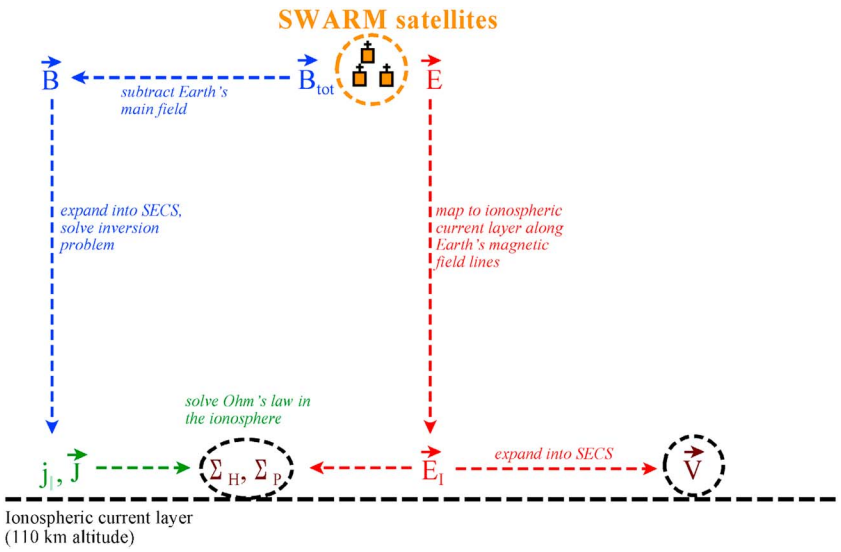

Figure 1. Schematic sketch of workflow for deriving maps of ionospheric electrodynamics parameters. The inversion problem mentioned on the left-hand side refers to inverting equation (2) for ***L***, while the expansion into SECS on the right-hand side refers to inverting equation (1) for ***I***.

One of the SECS vector basis functions is curl free everywhere and the other divergence free. Such basis functions can be superposed with different amplitudes, in order to reproduce any continuously differentiable vector field on the sphere. The amplitudes of the curl-free and divergence-free SECS basis functions are thus complete scalar representations of the vector field. One major advantage of this technique is that the analysis region can be freely chosen. For further details, we refer the reader to the literature as stated in section 1.

2.1. Maps of Ionospheric Parameters From Ionospheric Multispacecraft Data

In this paper, we concentrate on the case that is most relevant for the Swarm mission, namely, that two low-orbiting ionospheric satellites fly on parallel, polar orbits, with a zonal separation of the order of about 100 km in the auroral region. It should be noted that this technique can easily be extended if more satellites are available. For our study, we assume a thin sheet ionosphere with an ionospheric current layer at 110 km, where the resulting maps of ionospheric electrodynamics parameters will be derived.

The overall study logic of our technique is schematically shown in Figure 1. The Swarm electric field data are mapped to the ionospheric current layer along the magnetic field lines and there expanded into SECS. Thus, the ionospheric electric field, or equivalently the plasma flow, is calculated within a strip that envelops the trajectories of the two spacecraft. From the satellites' magnetic field data, first the Earth's main field contribution is subtracted. The remaining disturbance magnetic field is expanded into SECS, which allows direct calculation of the horizontal ionospheric sheet currents and field-aligned currents within the same strip. Finally, Ohm's law in the ionosphere is applied to calculate the Hall and Pedersen conductances from the electric field and the horizontal currents.

The geometry of the satellite orbits at auroral latitudes (as mentioned above, in accordance with the Swarm configuration here we use two satellites on polar orbits, flying parallel with a separation in zonal direction), the output area strip, and the region where 2-D SECS are applied is schematically shown in Figure 2. We analyze an arc of Swarm data of latitudinal length Θ, which is user definable. During the crossing of this arc length by the Swarm satellites, we assume the ionospheric situation to be stationary. The choice of Θ thus directly relates to the length of time for which this stationarity assumption is applied. For this section, we define the terms "meridional" as the direction along the median of the two parallel Swarm orbits and "zonal" as the direction perpendicular to it. The zonal arc length between the two parallel flying Swarm satellites (the black parallel lines in the figure) is Δ, which is defined by the spacecraft orbits and typically a function of latitude. The wanted meridional resolution of the results δ_{lat} is also user definable but shall not be smaller than the spatial resolution of the spacecraft data in meridional direction. The zonal resolution of the results is fixed at $\delta_{\mathrm{lon}} = \Delta/2$. We place a grid of 2-D SECS poles to this geometry with grid spacing δ_{lat} and δ_{lon}. The zonal

©2015. American Geophysical Union. All Rights Reserved.

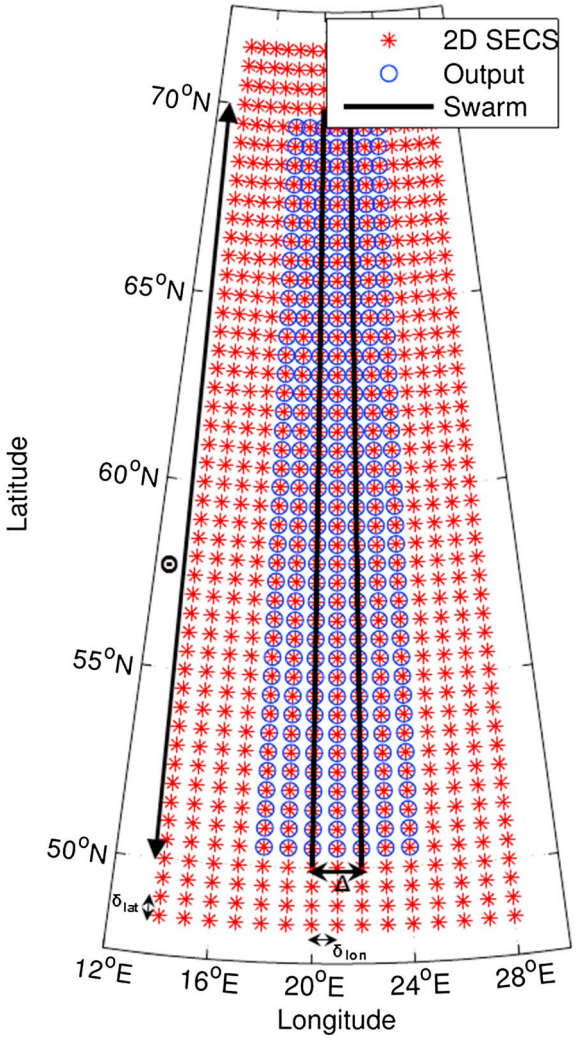

Figure 2. Sketch of geometry for ionospheric conductance study, showing the Swarm orbits (two black lines in the center), the output grid (blue circles), and the positions of the 2-D SECS poles (red asterisks). For more details, see the text.

extent of the grid is 7 Δ, and the meridional extent is $\delta_{\text{lat}} \times \text{Int}(\Theta/\delta_{lat}) + 8\ \delta_{\text{lat}}$, enabling the arc length Θ to be filled by 2-D SECS poles. Along both meridional borders, four rows of 2-D SECS poles are added. These 2-D SECS poles are marked by red asterisks in the figure. The geometry of the output grid where the conductances, currents, and electric field are calculated is similar to the 2-D SECS grid. However, the spatial extent is $\delta_{\text{lat}} \times \text{Int}(\Theta/\delta_{\text{lat}})$ in meridional direction, and 3 Δ in zonal direction. The output grid points are marked by blue circles in Figure 2. Moreover, 1-D SECS elementary systems are placed at the same latitudes as the central column of 2-D SECS (not shown in the figure). This technique of putting both 1-D and 2-D SECS we call "hybrid technique." It allows a more stable inversion than a plain 2-D SECS approach when the number of available spacecraft is small, because the 1-D SECS can describe any uniform background electrojet contribution with much less free parameters than the 2-D SECS alone. For each 1-D and 2-D SECS pole, both curl-free (cf) and divergence-free (df) SECS poles may be placed (depending on which parameter is to be calculated, see below).

Let the number of observation points of both Swarm satellites within the arc Θ be n, the number of all 1-D SECS poles be $m_{1\text{-D}}$, and the number of all 2-D SECS poles be $m_{2\text{-D}}$. Hence, we have n observation points $\boldsymbol{r}_i$, $i = 1, \ldots, n$ at which horizontal electric field observations $\boldsymbol{E}_i = (E_{i,\theta}, E_{i,\varphi})$ and magnetic field observations $\boldsymbol{B}_i = (B_{i,r}, B_{i,\theta}, B_{i,\varphi})$ exist. When using the SECS technique, implicitly the assumption of radial magnetic field lines is used (see paragraph "assumptions and limitations" below for a discussion on this), and since for this analysis only the horizontal electric field component is relevant, a possible radial component of the electric field is disregarded. We combine these data into the observation vectors $\boldsymbol{E} = (E_{1,\theta}, E_{1,\varphi}, E_{2,\theta}, E_{2,\varphi}, \ldots, E_{n,\theta}, E_{n,\varphi})$ and $\boldsymbol{B} = (B_{1,r}, B_{1,\theta}, B_{1,\varphi}, B_{2,r}, B_{2,\theta}, B_{2,\varphi}, \ldots, B_{n,r}, B_{n,\theta}, B_{n,\varphi})$. Thus, the vector $\boldsymbol{E}$ has $2n$ elements, and the vector $\boldsymbol{B}$ has $3n$ elements. After mapping radially down to the ionospheric current layer at 110 km altitude, the electric field at the current layer altitude is given at positions $\boldsymbol{r}'_i$, $i = 1, \ldots, n$, with same latitude and longitude components as $\boldsymbol{r}_i$, $i = 1, \ldots, n$, and the electric field at that altitude is given at these points as $\boldsymbol{E}' = \sqrt{B_l/B_{\text{Sat}}}\boldsymbol{E}$, where B_l is the absolute value of the background magnetic field at the level of the ionospheric current sheet, and B_{sat} the absolute value of the background magnetic field at the satellite level.

Using this geometry, we can first expand the electric field into SECS. Here we assume that any induced electric field component can be neglected, and thus, the electric field is curl free. Correspondingly, only curl-free (cf) 1-D and 2-D SECS are used in this step. The expansion into SECS then reads

$$\boldsymbol{E}' = \underline{\boldsymbol{M}}_{\boldsymbol{E}}\, \boldsymbol{I} \tag{1}$$

where $\boldsymbol{I} = (I_{\text{cf,1-D},1}, I_{\text{cf,1-D},2}, \ldots, I_{\text{cf,1-D},m1\text{-D}}, I_{\text{cf,2-D},1}, I_{\text{cf,2-D},2}, \ldots, I_{\text{cf,2-D},m2\text{-D}})$ is the vector of the 1-D and 2-D (curl-free) elementary system amplitudes which is the desired output quantity of the inversion of equation (1), and $\underline{\boldsymbol{M}}_{\boldsymbol{E}}$ is

©2015. American Geophysical Union. All Rights Reserved.

the geometry matrix containing the effect of *unit* 1-D and 2-D elementary systems (at positions $\theta_j, j = 1, \ldots, m_{1\text{-D}}$ for the poles of the 1-D systems whose effect only depends on latitude, and $\boldsymbol{r}''_k, k = 1, \ldots, m_{2\text{-D}}$ for the poles of the 2-D systems) to the θ and φ components of the electric field at the ionospheric positions $\boldsymbol{r}'_i, i = 1, \ldots, n$. Since this matrix only depends on the given geometry of the ionospheric and elementary system poles, it is known. Thus, together with the known $\boldsymbol{E}'$, we can invert equation (1) for the unknown vector $\boldsymbol{I}$. The technique used for the inversion is singular value decomposition (SVD) which effectively removes ill-conditioned parts of the inversion problem [*Amm and Viljanen*, 1999]. Once the elementary system amplitude vector $\boldsymbol{I}$ is known, the electric field $\boldsymbol{E}_{\text{Output}}$ can be calculated on the output grid using the general definition of the 1-D and 2-D SECS basis functions as given in *Amm* [1997], *Vanhamäki et al.* [2003], and *Juusola et al.* [2006].

In a similar way, the ionospheric horizontal currents and FAC are calculated from the satellites' magnetic field observations. Here we make use of the fact that we can analytically calculate the magnetic effect of a 1-D or 2-D SECS system at any point above (or below) the ionosphere, both for the "cf" and for the "df" systems [see *Amm and Viljanen*, 1999; *Juusola et al.*, 2006]. The expansion of the magnetic data into SECS then reads

$$\boldsymbol{B} = \underline{\boldsymbol{M}}_{\boldsymbol{B}} \boldsymbol{L} \tag{2}$$

where $\boldsymbol{L} = (L_{\text{cf,1-D,1}}, L_{\text{cf,1-D,2}}, \ldots, L_{\text{cf,1-D},m1\text{-D}}, L_{\text{cf,2-D,1}}, L_{\text{cf,2-D,2}}, \ldots, L_{\text{cf,2-D},m2\text{-D}}, L_{\text{df,1-D,1}}, L_{\text{df,1-D,2}}, \ldots, L_{\text{df,1-D},m1\text{-D}}, L_{\text{df,2-D,1}}, L_{\text{df,2-D,2}}, \ldots, L_{\text{df,2-D},m2\text{-D}})$ is the vector of the searched 1-D and 2-D elementary system amplitudes. Here we use the full set of curl-free (cf) and divergence-free (df) elementary systems. $\underline{\boldsymbol{M}}_B$ is the geometry matrix containing the effect of unit 1-D and 2-D elementary systems (at positions $\theta_j, j = 1, \ldots, m_{1\text{-D}}$ for the poles of the 1-D systems whose effect only depends on latitude, and $\boldsymbol{r}''_k, k = 1, \ldots, m_{2\text{-D}}$ for the poles of the 2-D systems) to the r, θ, and φ components of the magnetic field at the observation positions $\boldsymbol{r}_i, i = 1, \ldots, n$. Since this matrix only depends on the given geometry of the observations and elementary system poles, it is known. Again, together with the known $\boldsymbol{B}$, we can invert the above equation for the unknown vector $\boldsymbol{L}$ using the singular value decomposition (SVD) technique which effectively removes ill-conditioned parts of the inversion problem. Once the elementary system amplitude vector $\boldsymbol{L}$ is known, the ionospheric horizontal currents $\boldsymbol{J}$ can be calculated on the output grid using the general definition of the 1-D and 2-D SECS basis functions as mentioned above. The field-aligned currents $j_{\parallel}$ can then be computed by $j_{\parallel} = \text{div}_h \boldsymbol{J}$.

Once $\boldsymbol{E}_{\text{Output}}$ and $\boldsymbol{J}$ have been calculated, the ionospheric Hall and Pedersen conductances Σ_H and Σ_P can directly be computed on the output grid using Ohm's law in the ionosphere as

$$\Sigma_H = \left(\boldsymbol{J} \times \boldsymbol{E}_{\text{Output}}\right) / \left|\boldsymbol{E}_{\text{Output}}\right|^2 \tag{3}$$

and

$$\Sigma_P = \left(\boldsymbol{J} \cdot E_{\text{Output}}\right) / \left|\boldsymbol{E}_{\text{Output}}\right|^2 \tag{4}$$

Thus, we have achieved the calculation of ionospheric conductances on a strip around the two parallel Swarm orbits, as desired.

The following assumptions and limitations apply to this technique:

1. We assume that the electric field can be mapped from the satellite altitude to the altitude of the ionospheric current layer only by applying a geometry factor that accounts for the converging magnetic field lines. This means that the magnetic field lines are electric equipotentials, and that no polarization space charges should exist in between the two altitudes.
2. For the analytical equations that calculate the magnetic field of 1-D and 2-D SECS above (and below) the ionosphere [*Amm and Viljanen*, 1999; *Juusola et al.*, 2006], we use the assumption of radial magnetic field lines. Therefore, the analysis area should not include lower latitude areas where this assumption starts to cause significant errors. *Amm* [1999] estimated the lowest possible geomagnetic latitude where the error is still tolerable to about 45°.
3. We assume a stationary situation for the time that the Swarm satellites need to cover the arc length Θ. This arc length is, however, user definable. On the other hand, enough data points need to be gathered along Θ to make the inversion sensible. Tests have shown that for the case with two parallel flying satellites as discussed in this paper, $\Theta > 2°$ and $\Theta/\delta_{lat} \gtrsim 5$ should be applied.

©2015. American Geophysical Union. All Rights Reserved.

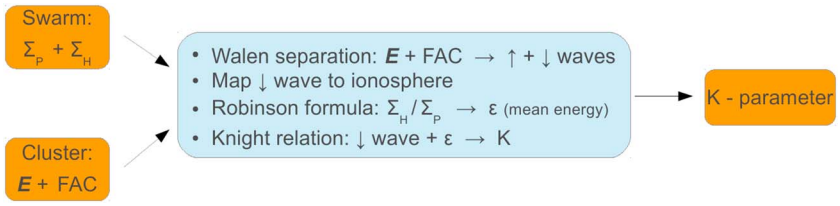

Figure 3. Schematic illustration of workflow for estimation of ionosphere-magnetosphere coupling parameter *K*.

4. The present technique does not automatically assure that the resulting conductances will always be positive (as they are in nature). Errors in the data, as well as numerical inaccuracies or the implicit extrapolation outside of the Swarm orbits where data values exist may locally lead to negative conductance values in the output grid.

2.2. Magnetosphere-Ionosphere Coupling Parameter *K*

In this section we briefly explain the workflow for the estimation of the ionosphere-magnetosphere coupling parameter *K*. This estimation requires that conjugate observations of the magnetospheric electric field and field-aligned currents (FAC) together with ionospheric low-orbiting multisatellite data are available. In this paper, we use the definition of the *K* parameter detailed in *Yoshikawa et al*. [2011],

$$j_{||}^{M \to I} = K \ (\Phi_I - \Phi_M). \tag{5}$$

Here Φ_I is the ionospheric electric potential, Φ_M is the magnetospheric electric potential, and $\boldsymbol{j}_{||}^{M \to I}$ is the part of the total FAC that is carried by the downgoing Alfvén wave, traveling from the magnetosphere toward the ionosphere. This definition is similar to the original definition of the *K* parameter given by *Knight* [1973], but in the original definition the total FAC are used on the left-hand side of equation (5). The division of the total FAC into its parts carried by an upgoing and a downgoing wave is performed by a Walén separation [*Walén*, 1944; *Yoshikawa et al*., 2011]. It should be noted that the part of FAC which is carried by a downward directed Alfvén wave should not be confused with downward directed currents. We also note that very similarly to the way described here, also the *K* parameter according to the original definition by *Knight* [1973] can be estimated, if so wished.

The workflow to estimate the *K* parameter is described below (see also the illustration in Figure 3, here with the Swarm and Cluster missions taken as examples). It is based on the ionospheric conductances estimated by our low-orbiting multisatellite analysis (see section 2.1), and on the conjugate magnetospheric data:

1. Calculate the Hall to Pedersen conductance ratio from the conductance results at the ionospheric footprint of the magnetospheric satellite(s), $\alpha = \Sigma_H / \Sigma_P$.
2. Calculate the average energy of the precipitating electrons to the ionosphere by $\alpha = 0.45\, E_{\mathrm{Average}}^{0.85}$ [*Robinson et al*., 1987].
3. Calculate the parallel potential drop between the ionosphere and the magnetosphere via $(\Phi_I - \Phi_M) = E_{\mathrm{Average}}/e$, where e is the charge of an electron.
4. Compute the total field-aligned currents $j_{||}$ at the conjugate magnetospheric satellite(s) using standard analysis techniques. (see, e.g., *Elphic et al*. [1985] and *Nagai* [1987] for single-spacecraft techniques and *Dunlop et al*. [2002] for a technique applicable to a magnetospheric multispacecraft mission such as Cluster.)
5. Compute the part of the FAC carried by Alfvén waves traveling from the magnetosphere to the ionosphere, $j_{||}^{M \to I}$, from the total FAC $j_{||}$ via a Walén separation, using the equations given by *Yoshikawa et al*. [2011].
6. Compute K via $j_{||}^{M \to I} = K\,(\Phi_I - \Phi_M)$.

In its reversed direction, a similar workflow has been used within MHD simulation schemes of the magnetosphere-ionosphere environment for estimating ionospheric conductances [*Zhang et al*., 2011]. In those schemes, typically E_{average} is derived from MHD parameters, such as plasma temperature. Here in contrast, the ionospheric conductances are estimated from the analysis as described in section 2.1 and input quantities.

©2015. American Geophysical Union. All Rights Reserved.

The assumptions used in our procedure are the following:

1. The empirical equation given in *Robinson et al*. [1987] is a reasonable description of the real situation. This equation has been derived for the condition of precipitating electrons into the ionosphere, as generally the case for upward FAC conditions. It is an open question how well the equation applies for situations with downward FAC. We note that the electron populations that are responsible for generation of ionospheric conductances, and those for carrying the FAC, are typically separate.
2. The velocity distribution of the electrons before acceleration is thermal.
3. The disturbance magnetic field (after subtraction of the background field) at the magnetospheric spacecraft is caused by field-aligned currents. This condition is best met if the magnetospheric spacecraft is located in the inner magnetosphere, where the influence of perpendicular currents is typically less significant.
4. The field-aligned currents at the magnetospheric spacecraft are carried by Alfvén waves. In fact, this is not really an assumption as any (field-aligned) current, even a constant one, can mathematically be described as a superposition of Alfvén waves.
5. The combination of ionospheric and magnetospheric conjugate data requires a magnetic field model, like, e.g., the one given by *Tsyganenko* [1989], in order to determine the conjugacy. Errors when using magnetic field models may lead to inaccuracies of the conjugacy determination. These errors are more critical for situations when the magnetospheric spacecraft is near its apogee than it is if the spacecraft is near its perigee.

These assumptions are standard assumptions that have been used in numerous previous research papers as well.

3. Model Applications

In this section, we test the performance of our new technique as described in section 2, using several synthetic situations of ionospheric and, for the K parameter estimation, also magnetospheric electrodynamics. We emphasize that our synthetic models are not meant to reproduce any specific situation of ionospheric and magnetospheric physics in any detail. Their purpose is solely to provide self-consistent and somewhat realistic test environments for examining the performance of our technique. Therefore, we neither dwell on specific features of the synthetic models here nor give a detailed description of the process of their generation. The models are self-consistent since they obey Ohm's law in the ionosphere, and current continuity. For the tests in this section, we use the case of two parallel flying low-orbiting satellites with polar orbits and a small zonal separation, as it is the case for which data are regularly available from the Swarm mission. We use an altitude of 400 km for this satellite pair.

3.1. Maps of Ionospheric Parameters From Ionospheric Multispacecraft Data

For each synthetic model case, the performance test logic of our new analysis technique is as follows:

1. Generate a self-consistent, synthetic model case, using simple analytical equations for the distributions of the (curl-free) ionospheric electric field and the ionospheric Hall and Pedersen conductances. Compute the resulting ionospheric horizontal currents from Ohm's law, and the FAC from the current continuity equation.
2. From the synthetic model, calculate the magnetic and electric fields at the satellites' orbits.
3. In order to mimic instrumental and processing errors, add white noise to the virtual data calculated in step 2. The magnitude of the white noise is chosen as 2% of the mean magnitude of the disturbance magnetic field, and 10% of the mean magnitude of the electric field, roughly taking into account different levels of expected precision of the respective instruments.
4. Use these synthetic data including noise along the two satellite orbits as input to our technique as described in section 2.1 and calculate the resulting maps of electric field, horizontal currents, FAC, Hall, and Pedersen conductance from it. The optimum truncation parameter ε in the SVD inversion method was chosen as in *Weygand et al*. [2011], by seeking that truncation point which minimizes the error in the resulting electric field and horizontal current maps when compared with the synthetic model.
5. Compare these results with the synthetic model distributions, and investigate the magnitude and distribution of errors.

Here we show two such synthetic test cases in detail: A decaying westward electrojet and a plasma convection vortex. The authors have studied a number of other test cases as well (not shown in this paper), with the overall performance of the technique being similar to the cases shown here.

©2015. American Geophysical Union. All Rights Reserved.

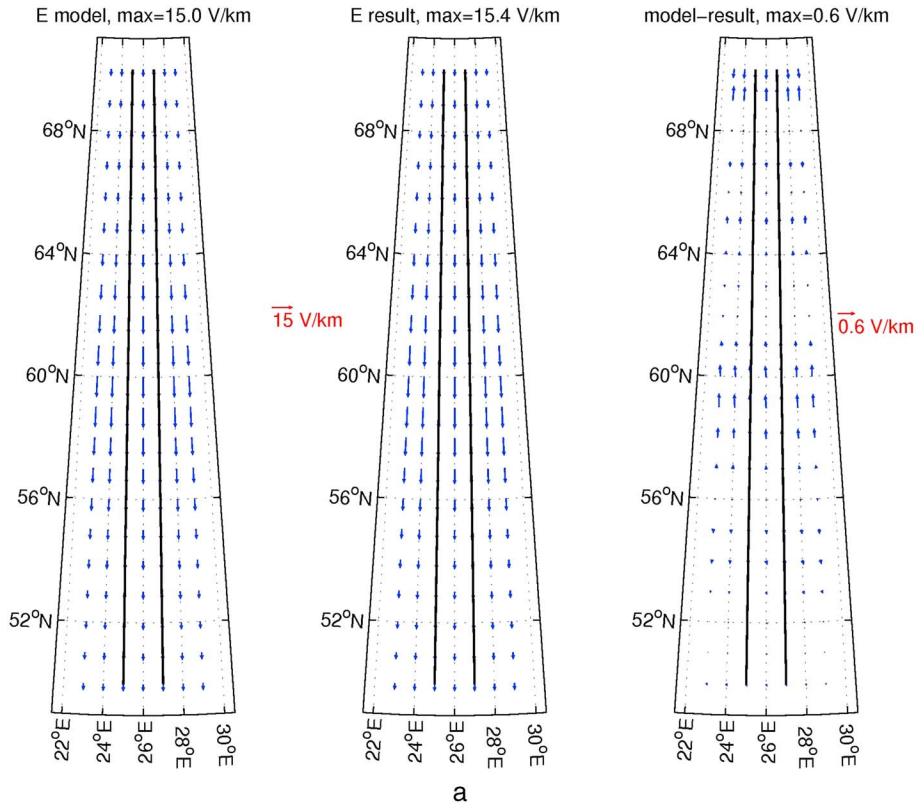

Figure 4. (a) Electric field maps for the test case of a decaying westward electrojet. (left) Original model distribution, (middle) output distribution of our new SECS-based analysis technique, using virtual spacecraft data along the two parallel satellite orbits (black lines) only, and (right) error map between model and output distributions. For better visibility, the density of the displayed vectors has been decreased as compared to the output resolution. (b) As in Figure 4a but for the Hall conductance. (c) As in Figure 4a but for the Pedersen conductance. (d) As in Figure 4a but for the horizontal ionospheric currents. (e) As in Figure 4a but for the field-aligned currents (FAC).

Figure 4 shows the test results for the decaying westward electrojet model. In this model, both ionospheric conductances have a significant zonal gradient over the spacecraft trajectories, such that the conductances are decreasing in the westward direction. For all figures in this section, the left panel shows the original model distribution, the middle panel shows the result of our analysis on the virtual spacecraft data including noise, as explained above, and the right panel shows the error, i.e., the difference between the result and the original models. Note that the scale for each panel is different, as indicated on top of the panels. This is particularly relevant to notice for the error plots, for which in most cases the scale is significantly smaller than that of the model and the analysis result plots. The spacecraft trajectories are indicated by the two black parallel lines.

For the decaying westward electrojet case, the model electric field (Figure 4a, left) is purely southward directed, and peaks at 15 mV/m in the center of the electrojet, located at 60° latitude. From there, it decreases both toward the poleward and equatorward directions. When looking at the resulting electric field map from our analysis (Figure 4a, middle), in spite of the noise we added to the virtual satellite data given along the two orbits, visually no difference to the model electric field can be perceived. The error map (Figure 4a, right) indeed reveals minor errors that are oscillating in latitudinal direction. At the electrojet center, the maximum error is around 4%. We note that the inversion procedure of equations (1) and (2) tries to optimize the solution over the whole analysis area, which means that errors exist also at the satellite tracks themselves, even though they tend to be smallest there.

The model Hall (Figure 4b, left) and Pedersen (Figure 4c, left) conductances peak in the electrojet's center at around ~30 S and ~15 S, respectively. These conductances then decay rapidly in both meridional directions. In addition to that, an even stronger gradient is applied in zonal direction, particularly for the Hall conductance.

©2015. American Geophysical Union. All Rights Reserved.

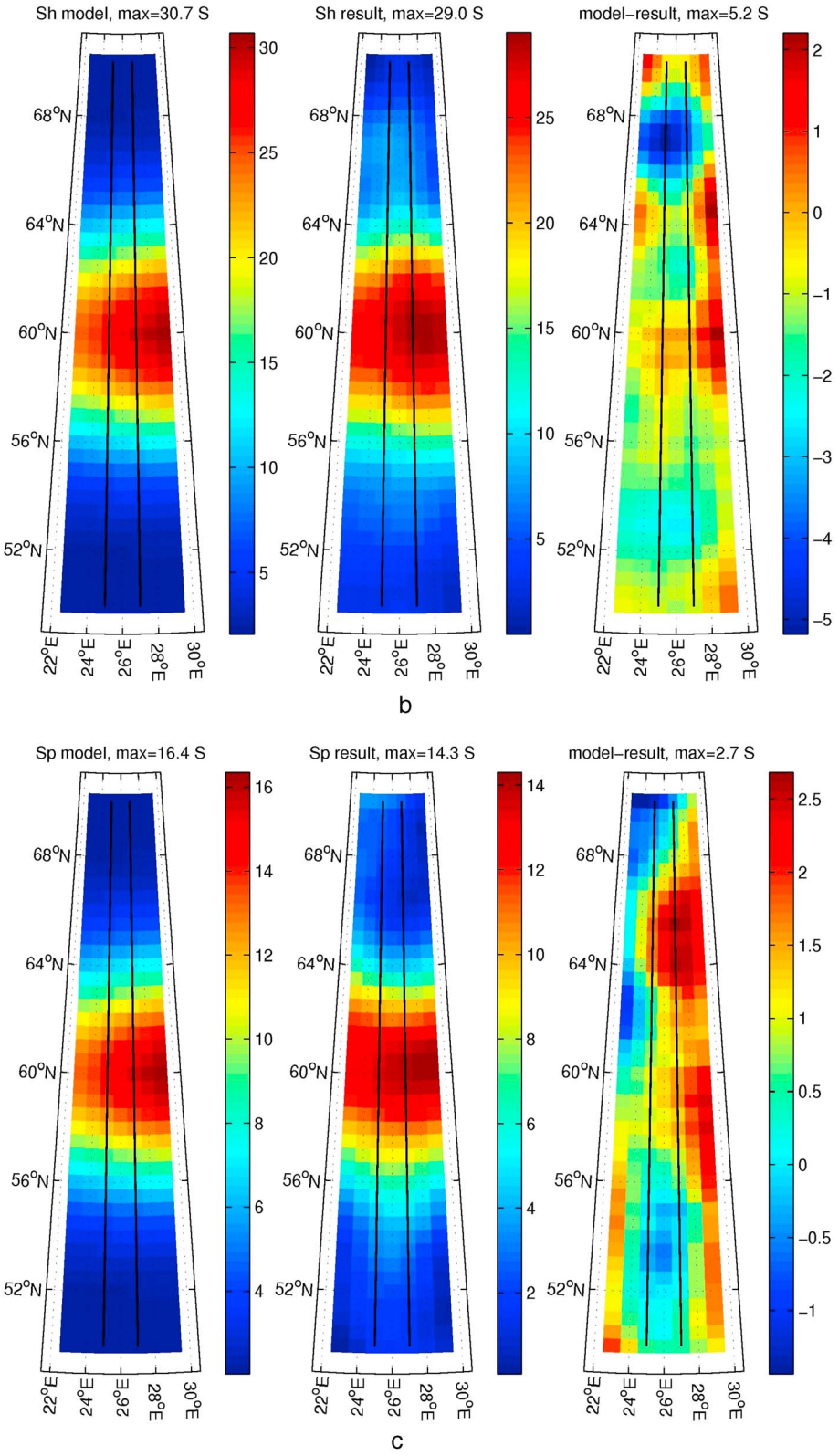

Figure 4. (continued)

©2015. American Geophysical Union. All Rights Reserved.

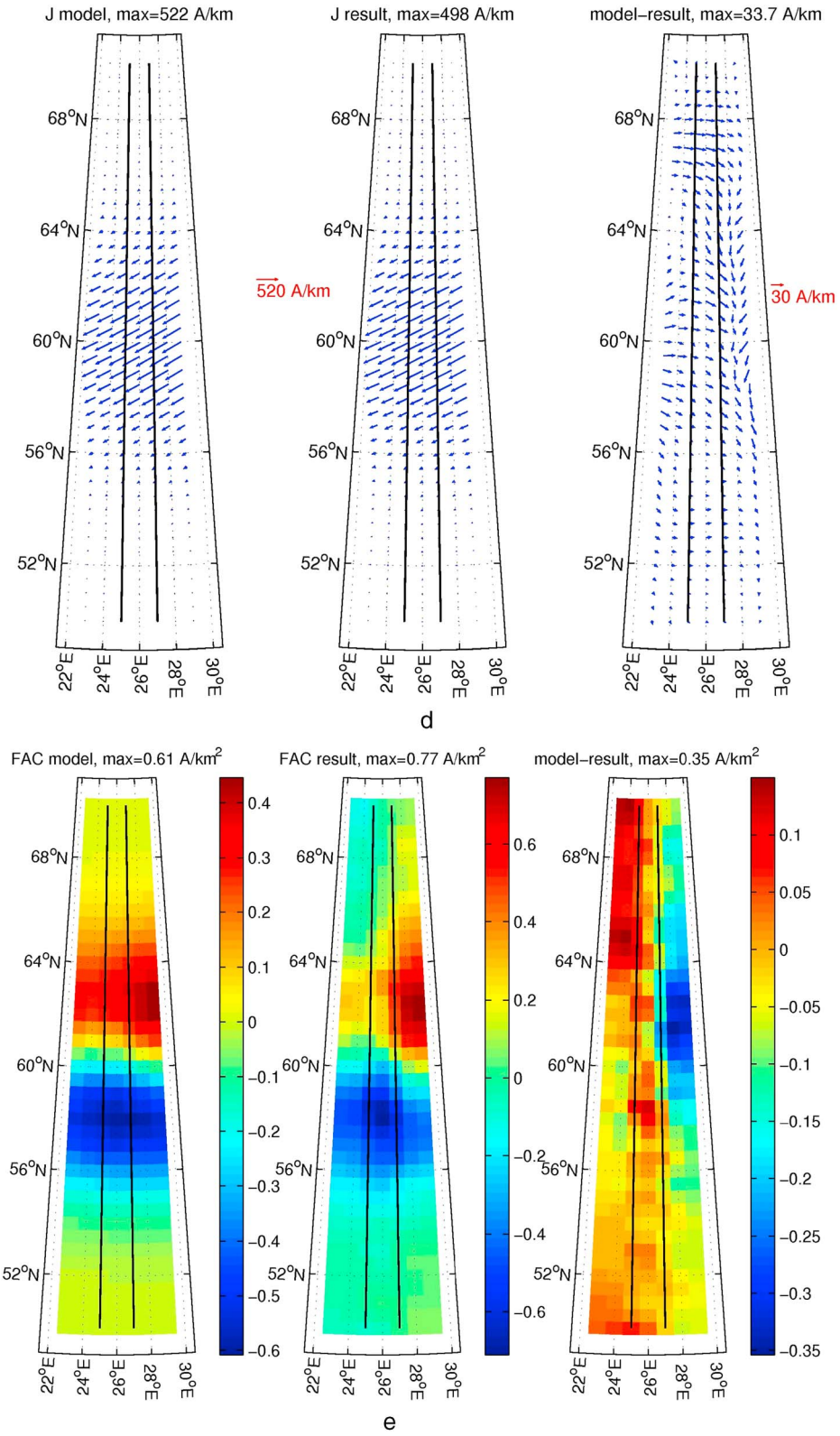

Figure 4. (continued)

©2015. American Geophysical Union. All Rights Reserved.

Note that the largest conductances are in both cases located eastward of both satellite orbits. In spite of that, the resulting Hall conductance map from our analysis (Figure 4b, middle) reconstructs the overall structure and magnitudes of the model Hall conductance distribution very well. In the area of the largest model Hall conductances, the relative error is about 6% or less. However, the decrease of the Hall conductance in westward direction is less steep in our results than in the model. Still, the absolute errors are less than 2 S, except for in a small area poleward of the electrojet where the model conductance is small. The reconstruction of the Pedersen conductance (Figure 4c, middle) is of similar accuracy: Again, the overall shape and magnitudes of the model distribution are very well preserved, but the zonal gradients, especially outside of the satellite orbits, is somewhat underestimated. Here the absolute errors are or the order of 2 S or less.

The resulting horizontal currents of our model (Figure 4d, left) are flowing in southwestward direction within the electrojet. The magnitude peaks in the central electrojet at ~500 mA/m, and decreases in both meridional and westward directions. Again, visually very little difference is perceived between the results of our analysis (Figure 4d, middle) and the model. The error map (Figure 4d, right), however, exhibits some deviations with relative errors of ~6% in the central electrojet region. The largest relative errors appear in the small area poleward of the electrojet where the Hall conductance results showed their largest errors. The absolute errors remain small at ~30 mA/m or less.

The model distribution of FAC (Figure 4e, left) shows two sheets of FACs: a downward FAC (positive values) poleward of the electrojet's center, and an upward FAC (negative values) equatorward of the electrojet's center, with a zonal gradient that reflects the gradients of the conductance distributions. For the spatial map of FAC, our analysis result (Figure 4e, middle) clearly exhibits the most substantial errors of all result maps. While the two FAC sheets are still recognizable, especially the zonal gradient of the poleward FAC sheet is largely overestimated, leading to relative errors of up to 50% at the western edge of that FAC sheet, outside of the two satellite orbits. The equatorward FAC sheet, on the other hand, is fairly well reconstructed with maximum relative errors of about 25%. The maximum absolute errors are ~0.35 A/km^2, which is a substantial error given the maximum FAC amplitude of the model to be ~0.6 A/km^2. It should be noted that although the horizontal currents and the FAC are related to each other via the current continuity equation, the horizontal currents are an integral of the FAC, which explains why their error is much less pronounced than the one of the FAC.

Our second test model consists of a current vortex with associated conductance enhancement. This model is composed as a particular challenge for our new analysis technique, in the sense that both the center of the vortex and of the conductance enhancement are located outside the two satellite trajectories along which input data for our technique exists. The model distributions, result maps, and error maps are shown in Figure 5, in the same style as for the decaying westward electrojet case.

The electric field of our plasma convection vortex model (Figure 5a, left) points toward the center of the vortex, which is located at 60° latitude, outside of our analysis region in the eastward direction. Its maximum magnitude is 20 mV/m. As in the decaying westward electrojet case, our analysis technique is able to reproduce the structure and overall also the magnitude of the electric field very well (Figure 5a, middle). However, the error map (Figure 5a, right) reveals a clear spatial differentiation of the error. While in the area between the satellite orbits and eastward of it, the errors are small and mostly in the range of magnitude like in the westward electrojet model, westward of the satellite orbits, and particularly along the western boundary of the analysis region, more significant errors of up to ~9 mV/m or up to ~45% are observed. These errors are largest at the latitude of the vortex' center and decrease longitudinally in both directions.

Our model comprises a circular enhancement of the Hall and Pedersen conductances around the center of the vortex (Figures 5b, left, and 5c, left), again with the most significant part of the enhancement situated eastward of the satellite orbits. Inside the analysis area, the Hall and Pedersen conductance reaches ~13 S and ~8 S, respectively. Despite the fact that most of the disturbance effect comes from outside the analysis area, our resulting Hall conductance map (Figure 5b, middle) reproduces remarkably well the shape and magnitude of the model Hall conductance distribution. Inside the strong conductance enhancement region eastward of the satellite orbits, errors are mostly of the order of 10% or less, and only around ~1 S in absolute values. However, the very sharp zonal conductance gradient of the model is not completely reproduced but somewhat smeared out, resulting in the largest error on the western border of the analysis region, around the latitude

©2015. American Geophysical Union. All Rights Reserved.

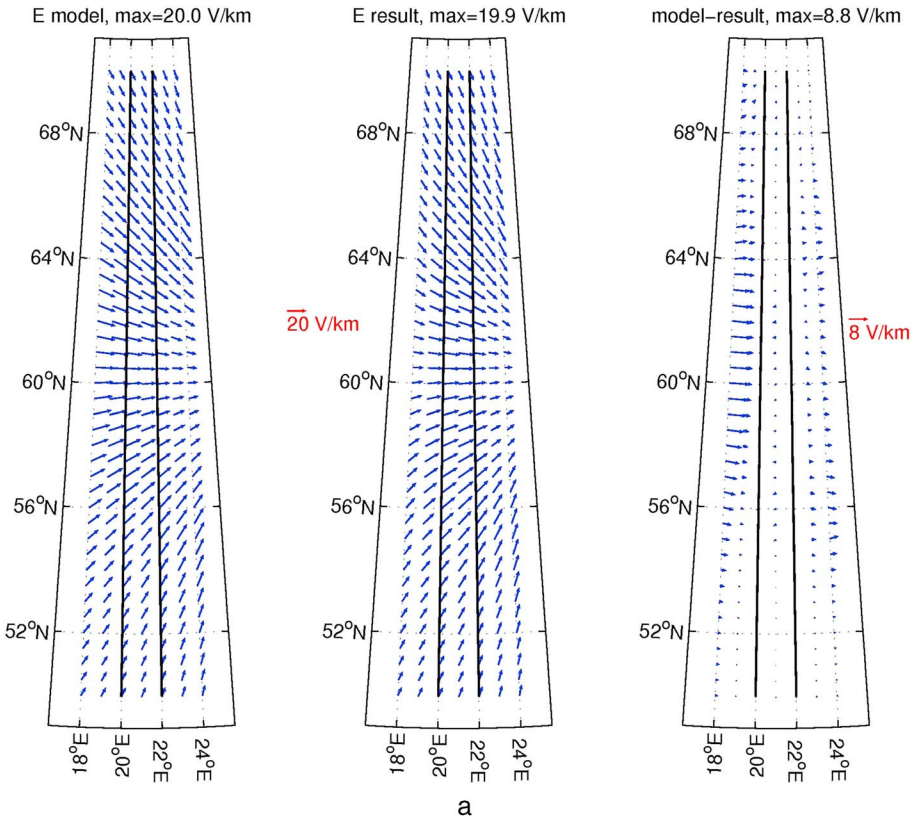

Figure 5. (a) Electric field maps for the test case of a vortex, the center of which being located in eastward direction outside of the analysis region. (left) Original model distribution; (middle) output distribution of our new SECS-based analysis technique, using virtual spacecraft data along the two parallel satellite orbits (black lines) only; and (right) error map between model and output distributions. (b) As in Figure 5a but for the Hall conductance. (c) As in Figure 5a but for the Pedersen conductance. (d) As in Figure 5a but for the horizontal ionospheric currents. (e) As in Figure 5a but for the field-aligned currents (FAC).

of the vortex's center. Here the absolute error has maximum values of ~4 S. This is due to the small model conductance leading to large relative errors of up to 75%. The resulting map for the Pedersen conductance (Figure 5c, middle) overall shows a similar behavior to that of the Hall conductance, but the errors at the western boundary change sign at the latitude of the vortex' center. Although they are with up to ~3 S in absolute values smaller than those of the Hall conductance, they reach even higher levels of relative error.

The horizontal currents of our vortex model (Figure 5d, left) exhibit a spiraling structure toward the center of the vortex, in the eastward direction outside of the analysis region. The current has a maximum strength of ~150 mA/m. Similar to the decaying westward electrojet case, also here the structure and magnitude of the current system is very well reproduced by our result map (Figure 5d, middle), with very little visually noticeable difference to the model distribution. Still, the error map (Figure 5d, right) shows some regions with larger errors up to ~50 mA/m or ~35%. These error vectors predominantly point into the direction of the model currents, or in the opposite direction, which is why they do not significantly distort the overall current pattern.

Again, by far the largest errors are encountered for the FAC distributions. The model FAC distribution (Figure 5e, left) consists of a circular area of upward FAC (negative values) around the vortex's center located outside of the analysis region. The maximum upward FAC density inside the analysis area is ~0.25 A/km^2. These upward FAC are balanced by a surrounding, larger area of small downward FAC. While the resulting map from our analysis (Figure 5e, left) reproduces this FAC structure very well, it strongly overestimates the upward FAC density at the eastern boundary of the analysis area, in the direction of the vortex's center. This overestimation reaches up to a factor of 2, or 100%. The reason for this is that while our

©2015. American Geophysical Union. All Rights Reserved.

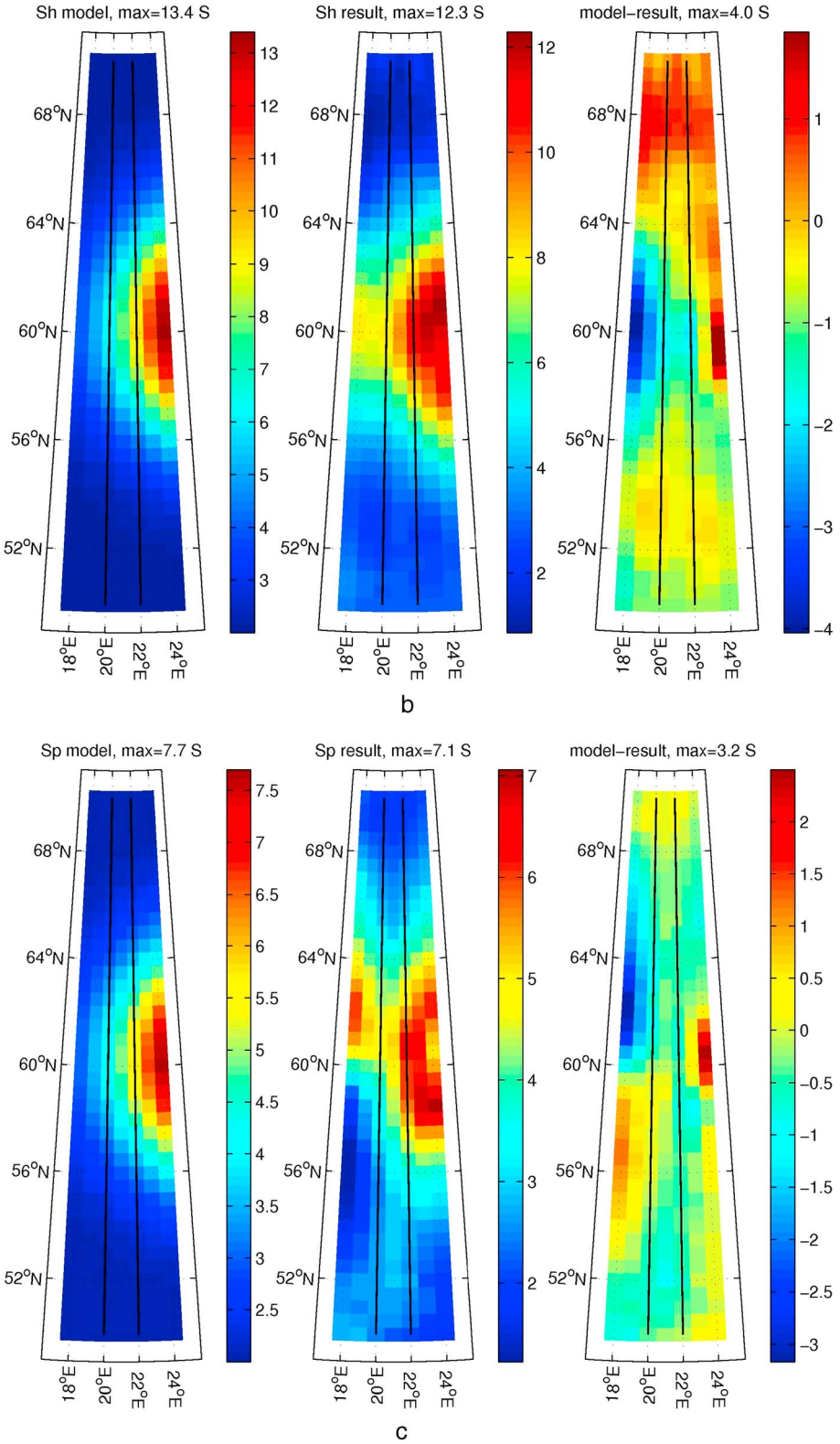

Figure 5. (continued)

©2015. American Geophysical Union. All Rights Reserved.

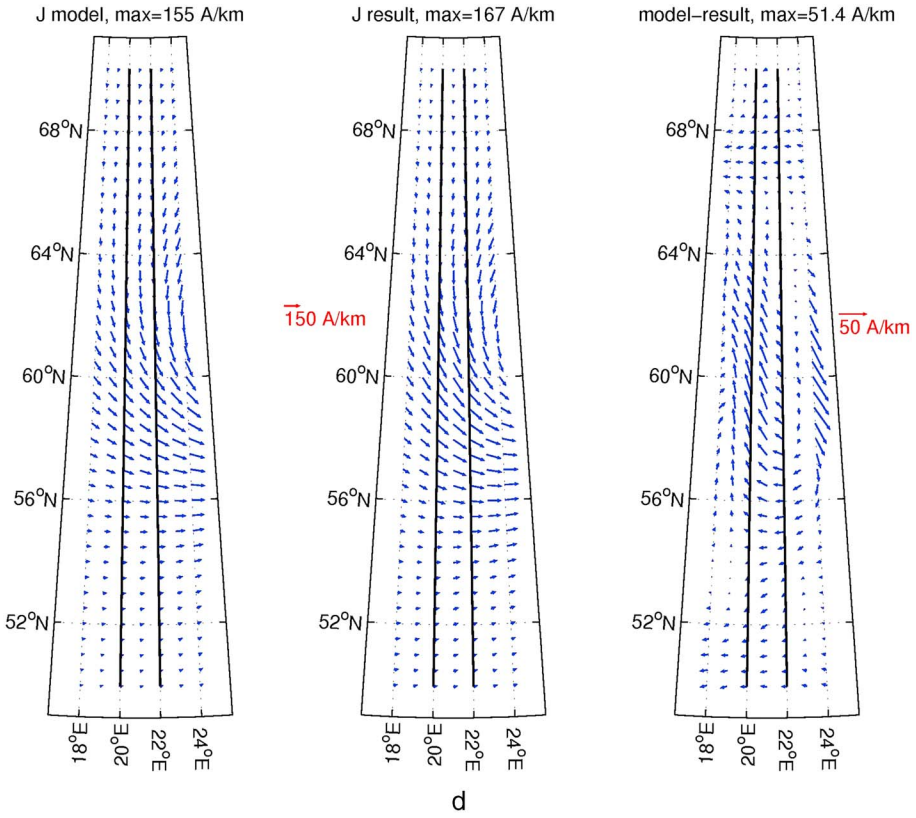

Figure 5. (continued)

©2015. American Geophysical Union. All Rights Reserved.

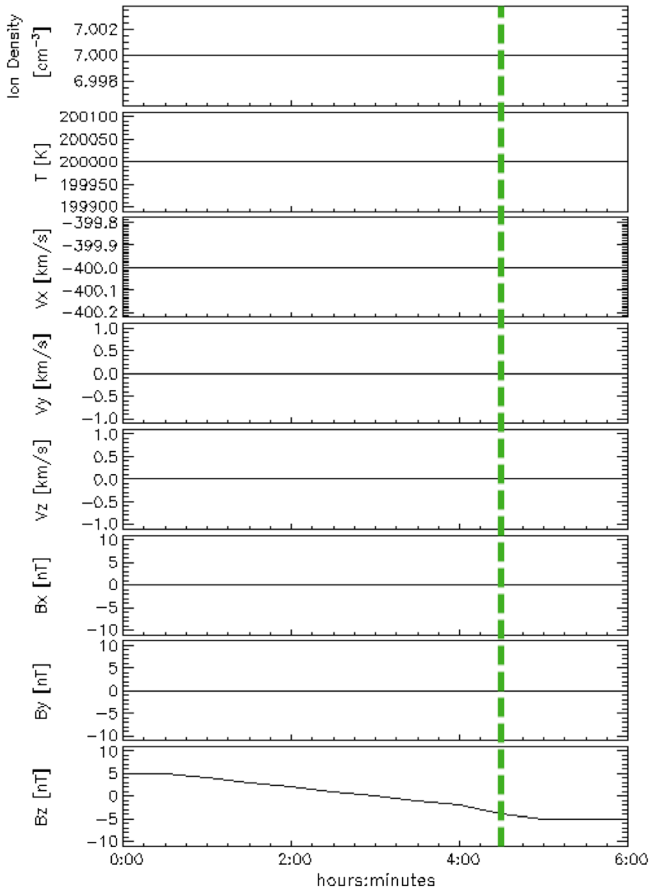

Figure 6. Input data for running the OpenGGCM simulation. (from top to bottom) Solar wind ion density, solar wind temperature, solar wind velocities in *X*, *Y*, and *Z* directions in geocentric solar magnetospheric (GSM coordinates), interplanetary magnetic field velocities in *X*, *Y*, and *Z* directions (GSM coordinates). The time axis refers to the simulation running time. The parameters in the upper seven panels are kept constant over the simulation.

technique can well estimate the structure and the integrated value of total FAC even outside the satellite orbits, there is no way to determine whether this integrated FAC effect stems from a region of concentrated FAC further away from the satellite orbits, or from a more distributed FAC region closer to the satellite orbit. The magnetic effect at the satellite orbit of the two cases is indeed identical. This is in fact not a limitation of our technique but a general consequence of the equivalence of different current systems with respect to their magnetic effect outside of those current systems. Here the inversion chooses to distribute the total FAC rather closely to the region outside the satellite orbits, which leads to an overestimation. We note that if we would add a third satellite track along the eastern border of our analysis area, this problem and the related errors disappear (results not shown). For example, such a configuration existed during the commissioning phase of the Swarm satellites, when all three spacecraft were flying side by side.

3.2. Magnetosphere-Ionosphere Coupling Parameter *K*

In this section, we are presenting a test case for the estimation scheme of the magnetosphere-ionosphere coupling parameter *K*, as presented in section 2.2. For this purpose, we need to generate a model data set that comprises both ionospheric low-orbiting satellite and conjugate magnetospheric satellite data, in an environment where both domains are self-consistently coupled with each other. We realize such an environment by a global magnetohydrodynamic (MHD) simulation run at the Community Coordinated Modeling Center located at NASA Goddard Space Flight Center. For the results presented here, we have used the OpenGGCM (Geospace General Circulation Model) [see *Raeder et al.*, 2001, and references therein]. This model includes a MHD simulation of the Earth's magnetosphere with an inner boundary at 4 R_E, and a coupled model of the ionosphere. In this case, conjugacy is determined by integrating the MHD model magnetic field in the magnetospheric domain, and following a dipole field between the inner boundary of the MHD domain and the ionosphere, as used in the OpenGGCM model.

The input parameters for our MHD simulation run are shown in Figure 6. As one can see, all parameters are kept constant except for the interplanetary magnetic field B_Z component, which changes through the simulation run from +5 nT to −5 nT. For the test case presented here, we use the snapshot of the OpenGGCM results in both the magnetosphere and the ionosphere at 0430 h of simulation running time (green vertical dashed line in Figure 6), which corresponds to a period of moderate activity in the Geospace environment. From this snapshot, we then calculate virtual data both of a magnetospheric multi-satellite mission, and of an ionospheric low-orbiting multisatellite mission. For the magnetospheric part, we use the actual positions of the four Cluster spacecraft [*Escoubet et al.*, 1999] on 27 June 2013 at 1036 UT. For the ionospheric part, we use

©2015. American Geophysical Union. All Rights Reserved.

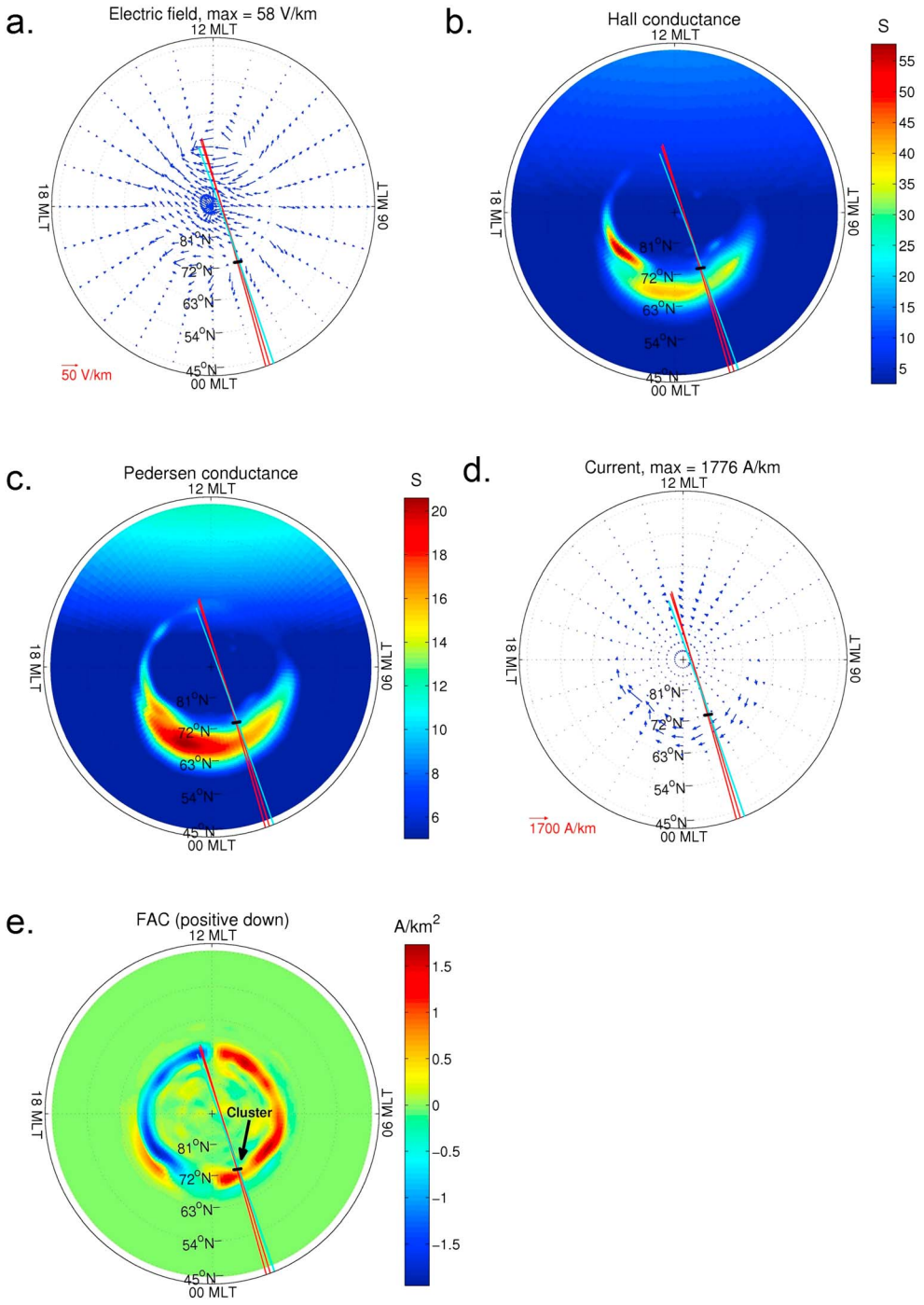

Figure 7. Ionospheric distributions of OpenGGCM output at 0430 h running time, together with virtual Swarm orbits (parallel red lines; the third Swarm orbit in cyan is not used here), and virtual Cluster 1 magnetic footprints (black line). (first panel) Electric field, (second panel) Hall conductance, (third panel) Pedersen conductance, (fourth panel) horizontal currents, and (fifth panel) field-aligned currents (FAC).

the same setup with two parallel flying satellites on polar orbits, referring to the Swarm constellation, as used in section 3.1. The location of the orbits of the ionospheric spacecraft is chosen to reach conjugacy with the Cluster spacecraft, here particularly with Cluster 1. Figure 7 shows the ionospheric state modeled by the OpenGGCM output at 0430 h of simulation time, together with the virtual Swarm orbits (red lines), and the ionospheric footprint of the virtual Cluster 1 satellite (short black line). The orbit of a third Swarm satellite (cyan) is not used

©2015. American Geophysical Union. All Rights Reserved.

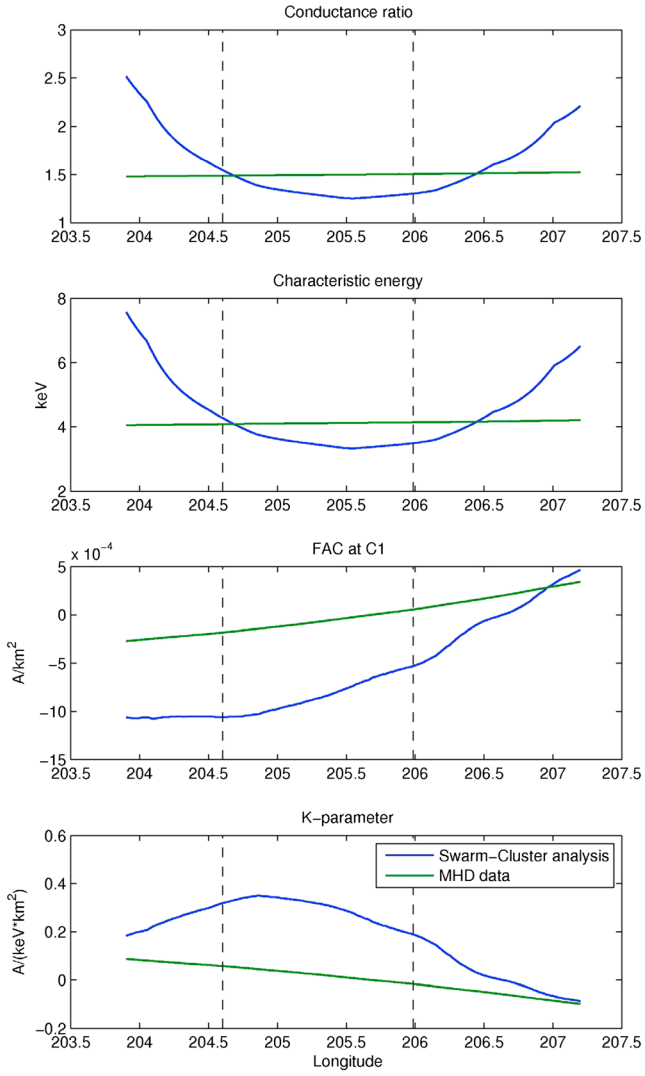

Figure 8. Comparison of original OpenGGCM model distributions (green lines) and output from combined virtual Swarm/Cluster analysis (blue lines) for magnetosphere-ionosphere coupling parameter K estimate. (first panel) Hall-to-Pedersen conductance ratio, (second panel) characteristic energy of precipitating electrons, (third panel) field-aligned currents (FAC) at Cluster 1 (part carried by downward Alfvén wave), and (fourth panel) *K* parameter.

here. As can be seen, the virtual Swarm/Cluster conjunction takes place in the early morning sector, poleward of the main westward electrojet, close to the velocity shear zone between equatorward electric fields in the auroral electrojet, and poleward electric fields in the polar cap. Once again, we emphasize that the particular details of this setup, both regarding geometry and the physical situation, are of no major interest for our purpose. We use the model here for the sole purpose of generating a self-consistent test environment for both our ionospheric and magnetospheric virtual data sets.

Since the MHD simulation does not directly give the ionosphere-magnetosphere coupling parameter *K* as an output, for our test of the *K* parameter estimate, we solve equation (5) twice: Either using directly the model data of the OpenGGCM simulation or by using the output of our new ionospheric multisatellite analysis technique and by calculating the magnetospheric FAC (and the part of it carried by the downward Alfvén wave) from the virtual Cluster magnetic field data. For the latter step, we here use the single-satellite approach (see introduction) with Cluster 1, and first apply the Walén separation to its magnetic field data, from which the field-aligned current is calculated. In practice, this approach has the advantage that it can be done for each Cluster satellite separately, allowing us to generate four nearby data sets for the *K* parameter estimate. The multisatellite approach, on the other hand, gives only one FAC data set from all four spacecraft but has the advantage of generally providing a more precise FAC estimation.

The results for the *K* parameter estimate using the original OpenGGCM model data are shown in green color in Figure 8 and are compared to those from our virtual Swarm and Cluster data analysis (blue color). The longitudes of the two virtual Swarm orbits are shown by vertical dashed lines in the plots. In between and around the Swarm orbits, our new ionospheric multisatellite data analysis technique is able to reproduce the model Hall to Pedersen conductance ratio well, with errors up to 20% or less (Figure 8, first panel). Outside of the Swarm satellite orbits, larger errors are seen. Accordingly, also the characteristic energy as calculated from the Hall to Pedersen conductance ratio using the relation given by *Robinson et al.* [1987] (Figure 8, second panel) is well estimated with a comparable error in the region between and around the Swarm satellite orbits. The largest error is actually introduced here by the single-satellite FAC estimation from the virtual Cluster 1 magnetic field data. Based on the actual MHD model data, the part of the FAC carried by the

©2015. American Geophysical Union. All Rights Reserved.

downward Alfvén wave (Figure 8, third panel) shows a moderate upward FAC at the conjunction point with the western Swarm satellite, which decreases to about zero at the conjunction point with the eastern satellite. Using the single-satellite FAC estimate on the Walén-separated magnetic field disturbance as observed by the virtual Cluster 1 data shows a similar overall trend of the FAC, but its magnitude is largely overestimated. These errors stem from the fact that in our test case, the Cluster 1 satellite passes through the FAC sheet at a very small angle, close to parallel, and in addition zonal gradients of FAC exist in that sheet. Consequently, the main error in the estimated *K* parameter values (Figure 8, fourth panel) is due to these inaccuracies of the magnetospheric FAC estimation. The *K* parameter as calculated from the original MHD model data decreases from about 0.1 at the western Swarm satellite to around 0 at the eastern satellite. While this decreasing trend is reproduced in the results from our virtual Swarm/Cluster analysis, the absolute values are too large, with ~0.3 at the western Swarm satellite to ~0.2 at the eastern one.

4. Summary and Conclusions

We have presented and tested a novel technique to generate maps of ionospheric electrodynamics parameters from magnetic and electric field data of low-orbiting ionospheric multispacecraft missions. We have further shown the logic how from the results of such an analysis, together with conjugate magnetospheric observations, we can estimate the ionosphere-magnetosphere coupling parameter *K*.

When designing a technique that attempts to reconstruct two-dimensional maps of ionospheric electrodynamics parameters from two lines of satellite data, it is clear that the results cannot be expected to be free of errors, nor to be unique, but should be seen in a "best fit to the data" sense. This is particularly important to keep in mind in when considering the areas outside of the satellite orbits. Nevertheless, as our test cases shown in section 3.1 demonstrate, the technique is able to reconstruct the modeled two-dimensional distributions with excellent to very good accuracy in between and even to some extent outside of the two low-orbiting spacecraft trajectories. For the electric field/convection, the Hall and Pedersen conductances, and the horizontal currents, in the relevant areas where significant activity exists, the relative errors are generally less than 10%. Larger relative errors show up in regions with small original model values of the ionospheric parameters, but also in these regions, absolute errors remain small. However, the resulting FAC maps exhibit more pronounced relative and absolute errors also in regions where significant activity exists. This is to be expected particularly outside of the satellite tracks, since different FAC configurations in these regions may result in the same magnetic field effect at the satellite orbits. Still, they reconstruct the general shape of the modeled FAC fairly well and give a good estimate of the integrated FAC (which is why the horizontal currents, the curl-free part of which is an integral of FAC shows much smaller errors). Qualitatively, similar results have been confirmed by several other test cases that the authors have examined (not shown in the paper).

When estimating the ionosphere-magnetosphere coupling parameter *K* using the workflow presented in section 2.2, there exist two sources of errors from the input data for equation (5): (i) The estimate of the Hall-to-Pedersen conductance ratio from the ionospheric analysis described in section 2.1 and (ii) the estimate of the field-aligned currents (and the part of it carried by the downward Alfvén wave) from the magnetospheric data. While conductance ratio estimation errors are moderate (at most 20%), much larger errors appear when estimating the FAC from magnetospheric data of a single virtual satellite. This latter procedure is not actually a part of the new technique presented in this paper, but a procedure that has been applied in the literature for many decades. Therefore, we do not consider optimizing this procedure as part of this study. In fact, in order not to be biased toward "perfect" events, we essentially randomly chose a Swarm-Cluster conjunction and ended up with an almost worst possible case for the single-satellite FAC estimate. We could easily have chosen a case where Cluster had crossed perfectly perpendicularly over a perfectly uniform current sheet, and the resulting FAC estimates would have been perfect as well. However, we chose to keep this test case in order to make the readers aware of the errors that may be related to that procedure. Nevertheless, the main point of this technique paper is to illustrate the way how the *K* factor can be derived, and in spite of the errors in the FAC estimate for this particular case, our results as shown in section 3.2 show that our technique provides, for the first time, the capability of inferring gradients of the *K* parameter solely from data.

In conclusion, the accuracy of the SECS-based reconstruction of maps of ionospheric parameters from low-orbiting, multisatellite data has proven sufficient for becoming a "standard product" of ionospheric

©2015. American Geophysical Union. All Rights Reserved.

multisatellite missions such as Swarm. This statement applies to maps of the ionospheric electric field/convection, Hall and Pedersen conductances, and ionospheric horizontal currents in the auroral region.

The FAC maps shall not be used for quantitative, pointwise studies, but rather as qualitative information for the structure of the FAC distribution and for its integrated value. *Ritter and Lühr* [2006] and *Ritter et al.* [2013] developed a curlometer-type technique that uses the magnetic field data of the two parallel Swarm spacecraft solely to determine the magnitude of FAC in between them. This technique, while limited in spatial coverage, provides FAC estimates of qualitatively higher precision. We note that this technique is conceptually similar to running our novel technique with just one line of SECS poles in between the two parallel spacecraft orbits.

While the ionospheric multisatellite data analysis technique as described above can be used as a "routine tool" whenever the satellites pass the auroral region, the estimate of the ionosphere-magnetosphere coupling parameter K requires in addition conjugate magnetospheric observations during the presence of an upward FAC region. It is thus suitable for event studies when these criteria are met. Specifically pertaining to the conjunctions between Swarm and the Cluster satellites, there will be about 450 conjunctions within 3 years which are suitable for applying the K parameter estimation as described here. In addition to errors from the ionospheric analysis, inaccuracies of the magnetospheric FAC estimation need to be taken into account. These inaccuracies may be diminished when using the magnetospheric curlometer technique as developed by *Dunlop et al.* [2002] with multisatellite missions such as Cluster. Despite of potential inaccuracies, this technique provides for the first time the opportunity to obtain gradients of the K parameter solely from data.

One of the main advantages of using the SECS technique for this purpose is that the shape of the analysis region can be freely chosen. *Fiori et al.* [2014] have applied the Spherical Cap Harmonic Analysis to synthetic Swarm electric field data. While they have shown that it is possible to apply these basis functions for producing electric field maps, a number of technical complications arise from the fact that the basis functions are defined on a spherical cap, but the data are given along a fairly narrow strip. We also mention that global models, or such that rely on statistical a priori information, are not applicable to the task described in this paper.

Acknowledgments

This work was conducted under a contract with the European Space Agency (ESA; ESTEC contract 4000106388/12/NL/BJ/lf), funded by the "Support To Science Element" (STSE) program. We would like to thank Aki Ieda (Nagoya University, Japan) for constructive comments on the paper. No data were used in the research for this manuscript.

Michael Balikhin thanks the reviewers for their assistance in evaluating this paper.

References

Amm, O. (1997), Ionospheric elementary current systems in spherical coordinates and their application, *J. Geomagn. Geoelectr.*, *49*(7), 947–955.

Amm, O. (1999), Method of characteristics in spherical geometry applied to a Harang-discontinuity situation, *Ann. Geophys.*, *16*(4), 413–424, doi:10.1007/s00585-998-0413-2.

Amm, O., and A. Viljanen (1999), Ionospheric disturbance magnetic field continuation from the ground to the ionosphere using spherical elementary current systems, *Earth Planets Space*, *51*(6), 431–440, doi:10.5636/eps.51.431.

Dunlop, M. W., A. Balogh, K.-H. Glassmeier, and P. Robert (2002), Four-point Cluster application of magnetic field analysis tools: The Curlometer, *J. Geophys. Res.*, *107*(A11), 1384, doi:10.1029/2001JA005088.

Elphic, R. C., P. A. Mutch, and C. T. Russell (1985), Observations of field-aligned currents at the plasma sheet boundary: An ISEE-1 and 2 survey, *Geophys. Res. Lett.*, *12*(10), 631–634, doi:10.1029/GL012i010p00631.

Escoubet, C. P., M. Fehringer, and M. Goldstein (1999), The Cluster mission, *Ann. Geophys.*, *19*(10/12), 1197–1200, doi:10.5194/angeo-19-1197-2001.

Fiori, R. A. D., D. H. Boteler, A. V. Koustov, D. Knudsen, and J. K. Burchill (2014), Investigation of localized 2D convection mapping based on artificially generated Swarm ion drift data, *J. Atmos. Sol. Terr. Phys.*, *114*, 30–41, doi:10.1016/j.jastp.2014.04.004.

Fujii, R., R. A. Hoffman, P. C. Anderson, J. D. Craven, M. Sugiura, L. A. Frank, and N. C. Maynard (1994), Electrodynamic parameters in the nighttime sector during auroral substorms, *J. Geophys. Res.*, *99*(A4), 6093–6112, doi:10.1029/93JA02210.

Fung, S. F., and R. A. Hoffman (1992), Finite geometry effects of field-aligned currents, *J. Geophys. Res.*, *97*(A6), 8569, doi:10.1029/91JA03026.

Iijima, T., and T. A. Potemra (1976), The amplitude distribution of field-aligned currents at northern high latitudes observed by Triad, *J. Geophys. Res.*, *81*(13), 2165–2174, doi:10.1029/JA081i013p02165.

Iijima, T., and T. A. Potemra (1978), Large-scale characteristics of field-aligned currents associated with substorms, *J. Geophys. Res.*, *83*(A2), 599–615, doi:10.1029/JA083iA02p00599.

Juusola, L., O. Amm, and A. Viljanen (2006), One-dimensional spherical elementary current systems and their use for determining ionospheric currents from satellite measurements, *Earth Planets Space*, *58*(5), 667–678.

Juusola, L., O. Amm, K. Kauristie, and A. Viljanen (2007), A model for estimating the relation between the Hall to Pedersen conductance ratio and ground magnetic data derived from CHAMP satellite statistics, *Ann. Geophys.*, *25*(3), 721–736, doi:10.5194/angeo-25-721-2007.

Knight, S. (1973), Parallel electric fields, *Planet. Space Sci.*, *21*, 741–750, doi:10.1016/0032-0633(73)90093-7.

Nagai, T. (1987), Field-aligned currents associated with substorms in the vicinity of synchronous orbit: 2. GOES 2 and GOES 3 observations, *J. Geophys. Res.*, *92*(A3), 2432–2446, doi:10.1029/JA092iA03p02432.

Olsen, N. (1996), A new tool for determining ionospheric currents from magnetic satellite data, *Geophys. Res. Lett.*, *23*(24), 3635–3638, doi:10.1029/96GL02896.

Olsen, N., et al. (2013), The Swarm Satellite Constellation Application and Research Facility (SCARF) and Swarm data products, *Earth Planets Space*, *65*(11), 1189–1200, doi:10.5047/eps.2013.07.001.

Raeder, J., R. L. McPherron, L. A. Frank, S. Kokubun, G. Lu, T. Mukai, W. R. Paterson, J. B. Sigwarth, H. J. Singer, and J. A. Slavin (2001), Global simulation of the Geospace Environment Modeling substorm challenge event, *J. Geophys. Res.*, *106*(A1), 381–395, doi:10.1029/2000JA000605.

©2015. American Geophysical Union. All Rights Reserved.

Reigber, C., H. Lühr, and P. Schwintzer (2002), CHAMP mission status, *Adv. Space Res.*, *30*(2), 129–134, doi:10.1016/S0273-1177(02)00276-4.
Rich, F. J., and M. S. Gussenhoven (1987), The absence of region 1/Region 2 field-aligned currents during prolonged quiet times, *Geophys. Res. Lett.*, *14*(7), 689–692, doi:10.1029/GL014i007p00689.
Ritter, P., and H. Lühr (2006), Curl-B technique applied to Swarm constellation for determining field-aligned currents, *Earth Planets Space*, *58*, 463–476.
Ritter, P., H. Lühr, A. Viljanen, O. Amm, A. Pulkkinen, and I. Sillanpää (2004), Ionospheric currents estimated simultaneously from CHAMP satellite and IMAGE ground-based magnetic field measurements: A statistical study at auroral latitudes, *Ann. Geophys.*, *22*(2), 417–430, doi:10.5194/angeo-22-417-2004.
Ritter, P., H. Lühr, and J. Rauberg (2013), Determining field-aligned currents with the Swarm constellation mission, *Earth Planets Space*, *65*(11), 1285–1294, doi:10.5047/eps.2013.09.006.
Robinson, R. M., R. R. Vondrak, K. Miller, T. Dabbs, and D. Hardy (1987), On calculating ionospheric conductances from the flux and energy of precipitating electrons, *J. Geophys. Res.*, *92*(A3), 2565–2569, doi:10.1029/JA092iA03p02565.
Tsyganenko, N. A. (1989), A magnetospheric magnetic field model with a warped tail current sheet, *Planet. Space Sci.*, *37*(1), 5–20, doi:10.1016/0032-0633(89)90066-4.
Vanhamäki, H., and O. Amm (2011), Analysis of ionospheric electrodynamic parameters on mesoscales—A review of selected techniques using data from ground-based observation networks and satellites, *Ann. Geophys.*, *29*(3), 467–491, doi:10.5194/angeo-29-467-2011.
Vanhamäki, H., O. Amm, and A. Viljanen (2003), One-dimensional upward continuation of the ground magnetic field disturbance using spherical elementary current systems, *Earth Planets Space*, *55*(10), 613–625.
Walén, C. (1944), On the theory of sunspots, *Ark. Mat. Astron. Fys.*, *31*(3), 1–87.
Weygand, J. M., O. Amm, A. Viljanen, V. Angelopoulos, D. Murr, M. J. Engebretson, H. Gleisner, and I. Mann (2011), Application and validation of the spherical elementary currents systems technique for deriving ionospheric equivalent currents with the North American and Greenland ground magnetometer arrays, *J. Geophys. Res.*, *116*, A03305, doi:10.1029/2010JA016177.
Yoshikawa, A., O. Amm, H. Vanhamäki, and R. Fujii (2011), A self-consistent synthesis description of magnetosphere-ionosphere coupling and scale-dependent auroral process using shear Alfvén wave, *J. Geophys. Res.*, *116*, A08218, doi:10.1029/2011JA016460.
Zhang, B., W. Lotko, M. J. Wiltberger, O. J. Brambles, and P. A. Damiano (2011), A statistical study of magnetosphere–ionosphere coupling in the Lyon–Fedder–Mobarry global MHD model, *J. Atmos. Sol. Terr. Phys.*, *73*(5–6), 686–702, doi:10.1016/j.jastp.2010.09.027.
Zmuda, A. J., and J. C. Armstrong (1974), The diurnal flow pattern of field-aligned currents, *J. Geophys. Res.*, *79*(31), 4611–4619, doi:10.1029/JA079i031p04611.

©2015. American Geophysical Union. All Rights Reserved.